Dependence of electron density on Fermi energy in compensated *n*-type gallium antimonide

Herbert S. Bennett[a)]
Semiconductor Electronics Division, National Institute of Standards and Technology, Gaithersburg, Maryland 20899

Howard Hung
Mathematical and Computational Sciences Division, National Institute of Standards and Technology, Gaithersburg, Maryland 20899

Alan Heckert
Statistical Engineering Division, National Institute of Standards and Technology, Gaithersburg, Maryland 20899

(Received 19 April 2005; accepted 13 October 2005; published online 30 November 2005)

The majority electron density as a function of the Fermi energy is calculated in zinc blende, compensated *n*-type GaSb for donor densities between 10^{16} and 10^{19} cm^{-3}. The compensation acceptor density is 10^{16} cm^{-3}. These calculations solve the charge neutrality equation self-consistently for a four-band model (three conduction subbands at Γ, L, and X and one equivalent valence band at Γ) of GaSb. Our calculations assume parabolic densities of states and thus do not treat the density-of-states modifications due to high concentrations of dopants, many-body effects, and nonparabolicity of the bands. Even with these assumptions, the results are important for interpreting optical measurements such as Raman scattering measurements that are proposed as a nondestructive method for wafer acceptance tests. [DOI: 10.1063/1.2134878]

I. INTRODUCTION

Microelectronics and nanomaterials technology roadmaps all call for nondestructive and fast-turn around methods to measure the optical and transport properties such as carrier concentrations in semiconductor wafers and epitaxial layers.[1–3] Manufacturers want to use these methods to determine whether semiconductor wafers and epitaxial layers meet specifications and are worthy of further processing. The nondestructive methods become economically more significant for III-V compound semiconductor wafers and epitaxial layers such as GaSb because these wafers and their epitaxial layers are more expensive per unit area than Si-based wafers and epitaxial layers. Measurement methods that require contacts may be acceptable for Si-based wafers, but such destructive methods are much less acceptable for III-V compound semiconductor based wafers and epitaxial layers. Also, the regions of wafers used for making contacts cannot be used for product.

The carrier concentration is a key figure of merit associated with a go-no-go decision for determining whether a wafer or an epilayer meets specifications and should undergo further processing. Raman spectroscopy is proposed as one possible way to measure nondestructively carrier concentrations.[4] The shape of the Raman spectral lines due to the longitudinal-optic phonons interacting with the plasmon collective modes of the electron gas (the so-called coupled LO phonon-plasmon Raman modes) provides information on transport properties of the electron gas.[4–9] The frequencies ω of the coupled modes are proportional to carrier concentrations and the peak widths $\Delta\omega$ of the coupled modes are proportional to the scattering rates due to electron-phonon interactions. The qualitative determination of carrier concentration and mobility, which is inversely proportional to the scattering rate, from Raman spectra is reasonably straightforward based on these proportionalities. The quantitative determination of carrier concentrations and mobilities requires more sophisticated modeling of the spectra. Many of these models involve fitting the spectra with the Fermi energy as a parameter and then determining the carrier concentration from knowing the fitted Fermi energy.[4–9]

Most interpretations of Raman spectroscopic measurements on compound semiconductors such as GaSb require physical models and associated input parameters that describe how carrier densities vary with dopant concentrations, band structure, and Fermi energies. Other researchers have investigated physical models for the conduction band of GaSb in the context of Hall-mobility and magnetoresistance measurements.[10–13] In this paper, we emphasize physical models for the conduction band of GaSb in the context of interpreting Raman measurements as a nondestructive and noncontacting technique to assess wafer quality. Using a higher level of theoretical rigor for GaSb than prior work, we report on a method that gives closed-form analytic expressions for the carrier densities in the conduction subbands for compensated *n*-type GaSb at room temperature as functions of the Fermi energy and summarize our results in forms that are convenient for other researchers to access. The method is based on an iterative and self-consistent solution of the charge neutrality equation with full Fermi-Dirac statistics for

[a)]FAX: 301-975-6021; electronic mail: herbert.bennett@nist.gov

Downloaded 11 Mar 2008 to 129.6.65.17. Redistribution subject to AIP license or copyright; see http://jap.aip.org/jap/copyright.jsp

the carriers at finite temperature and on the use of statistical analyses to give closed-form analytic expressions that represent the theoretical calculated data sets.

The method reported here is related to earlier work on uncompensated n-type GaAs and GaSb.[14,15] Reference 14 gives the results predicted by an effective two-band model, one equivalent conduction band and one equivalent valence band at Γ, that includes the densities-of-states modifications due to high concentrations of dopants and due to many-body effects associated with carrier-carrier interactions. Reference 15 describes a four-band model for uncompensated GaSb. Unlike Ref. 14, Ref. 15 and this paper do not include the densities-of-states modifications due to high concentrations of dopants and due to many-body effects because of computational limitations.

II. THEORY

The electron n and hole h concentrations in units of cm^{-3} at thermal equilibrium are given, respectively, by

$$n = \int_{-\infty}^{+\infty} f_0(E)\rho_c(E)dE \text{ and } h = \int_{-\infty}^{+\infty} [1 - f_0(E)]\rho_v(E)dE, \tag{1}$$

where $f_0(E)=\{1+\exp[(E-E_F)/k_BT]\}^{-1}$ is the Fermi-Dirac distribution function, E_F is the Fermi energy in eV, $\rho_c(E)$ and $\rho_v(E)$ are, respectively, the electron density of states for the conduction band and the hole density of states for the valence band, k_B is the Boltzmann constant, and T is the temperature in Kelvin. The calculations incorporate the Thomas-Fermi expression for the screening radius,

$$r_s^2 = -\frac{4\pi e^2}{\varepsilon\varepsilon_0}\int_{-\infty}^{+\infty} \frac{df_0(E)}{dE}[\rho_c(E) - \rho_v(E)]dE, \tag{2}$$

and the charge neutrality condition

$$N_I = n - h, \tag{3}$$

to compute self-consistently the Fermi energy E_F and the screening radius r_s for given values of the ionized dopant concentration N_I and temperature T. The static dielectric constant is ε and the permittivity of free space is ε_0. The ionized dopant concentration is positive for n-type material (donor ions) and negative for p-type material (acceptor ions). The results reported here are for the compensated n-type material, for which the donor density N_D is greater than the acceptor density N_A and $N_I=N_D-N_A\geqslant 0$. The results for the screening radius r_s are not reported here because they are not needed to extract the carrier concentrations from Raman scattering measurements.

In this paper, we use the four-band model that has three conduction subbands centered at the Γ, L, and X symmetry points in the Brillouin zone and one equivalent valence band centered at the Γ symmetry point. We do not include the detailed nonparabolicity of the GaSb energy bands at Γ. Unlike GaAs, the GaSb conduction Γ, L, and X subband masses and energy spacings are such that the conduction subband at L is the most populated one for donor densities of technological interest. The nonparabolicity of the conduction Γ subband in GaAs is discussed in Ref. 16. If we were to use the Kane three-level $k\cdot p$ model,[16] which does not include the conduction subbands at L and X, we would be able to include the nonparabolicity of the conduction Γ subband. However, because the conduction Γ subband in GaSb is not the dominant band for determining the Fermi energy, its nonparabolicity correction may not have a significant effect on the results given below and may lie within the uncertainties associated with the band masses quoted in the literature for GaSb.

TABLE I. Coefficients for the temperature dependence of the conduction band extrema that are used in Eq. (5). These data are from Ref. 17.

Parameter	Symbol	Value	Units
Γ subband	$E_{\Gamma 0}$	0.813	eV
Γ subband	A_Γ	3.78×10^{-4}	eV/K
Γ subband	B_Γ	94	K
L subband	E_{L0}	0.902	eV
L subband	A_L	3.97×10^{-4}	eV/K
L subband	B_L	94	K
X subband	E_{X0}	1.142	eV
X subband	A_X	4.75×10^{-4}	eV/K
X subband	B_X	94	K

The heavy-hole mass m_{hh} and light-hole mass m_{lh} for the two degenerate subbands at the top of the valence band are combined to give an effective mass

$$m_{v\Gamma} = (m_{hh}^{3/2} + m_{lh}^{3/2})^{2/3}, \tag{4}$$

for the valence topmost subband.

The zero of energy is at the bottom of the conduction Γ subband. The bottoms of the conduction L and X subbands are, respectively, at E_{cL} and E_{cX}. The top of the degenerate valence Γ subband is at $-E_G$, where E_G is the band gap of GaSb. The split-off valence subband at Γ due to spin-orbit coupling and the nonparabolicity factor of the conduction Γ subband are neglected. The probabilities for typical carriers in equilibrium to occupy appreciably these states are low. This means that the Fermi energies should be sufficiently above the valence subband maximum at Γ. Placing exact limits on the Fermi energies for which the four-band model is valid would be tenuous, because knowledge of how the various subbands move relative to one another due to the dopant concentrations considered here and due to many-body effects is not adequate.

The general expression[17] for the temperature dependence of conduction subband minima relative to the top of the valence band at Γ is

$$E_i = E_{i0} - [A_i T^2/(T + B_i)] \tag{5}$$

in units of eV, where $i=\Gamma$, L, or X. A consensus among researchers for the values to use for E_{i0}, A_i, and B_i does not appear to exist. The values from Ref. 17 for the coefficients E_{i0}, A_i, and B_i are listed in Table I and are the values we use in this paper. At 300 K, the coefficients in Table I give the following values for the subband minima: $E_{\Gamma 0}=0.726$ eV, $E_{L0}=0.810$ eV, and $E_{X0}=1.036$ eV. Whereas, the values for the coefficients E_{i0}, A_i, and B_i listed in Table VII of Ref. 18 give the following values for the subband minima at 300 K:

Downloaded 11 Mar 2008 to 129.6.65.17. Redistribution subject to AIP license or copyright; see http://jap.aip.org/jap/copyright.jsp

TABLE II. Input parameters for intrinsic zinc-blende GaSb at 300 K. The energies of the extrema of the conduction and valence subbands are referenced to the bottom of the conduction subband at the Γ symmetry point in the Brillouin zone of the reciprocal lattice space. The mass of the free electron is m_0. These data are from Ref. 17.

Parameter	Symbol	Value	Units
Lattice constant	a_L	$6.095\,93\times10^{-8}$	cm
Dielectric constant in vacuum	ε	8.854×10^{-12}	F/m
Static dielectric constant	ε_0	15.7	
Band gap	$E_G=\|E_{v\Gamma}\|$	0.726	eV
Bottom of the conduction L subband	E_{cL}	0.084	eV
Bottom of the conduction X subband	E_{vX}	0.31	eV
Top of the degenerate valence Γ subband	$-E_{v\Gamma}$	−0.726	eV
Spin-orbit splitting	E_{so}	0.80	eV
Top of the split-off (spin-orbit splitting) valence Γ subband	$-E_{so\Gamma}=-E_{v\Gamma}-E_{so}$	−1.526	eV
Effective mass of conduction Γ subband	$m_{c\Gamma}$	0.041	m_0
Transverse L subband mass	m_{tL}	0.11	m_0
Longitudinal L subband mass	m_{lL}	0.95	m_0
Effective mass of conduction L subband	$m_{cL}=(m_{lL}m_{tL}^2)^{1/3}$	0.226	m_0
Transverse X subband and mass	m_{tX}	0.22	m_0
Longitudinal X subband mass	m_{lX}	1.51	m_0
Effective mass of conduction X subband	$m_{cX}=(m_{lX}m_{tX}^2)^{1/3}$	0.418	m_0
Light-hole mass of degenerate valence Γ subband	m_{lh}	0.05	m_0
Heavy-hole mass of degenerate valence Γ subband	m_{hh}	0.4	m_0
Effective mass of degenerate valence Γ subband	$m_{v\Gamma}$	0.41	m_0
Split-off band mass of the valence subband at Γ	m_{so}	0.14	m_0
Number of equivalent conduction L subbands	N_{cL}	4	
Number of equivalent conduction X subbands	N_{cX}	3	

$E_{\Gamma0}=0.727$ eV, $E_{L0}=0.753$ eV, and $E_{X0}=1.033$ eV. There is good agreement for $E_{\Gamma0}$ and E_{X0} between Refs. 17 and 18 and the values for E_{L0} agree to within 8%. This 8% variation in the fitted values of E_{L0} is reasonable because there is a spread of from 10% to 20% in the experimental values of E_{L0}.[18]

The general expression for the parabolic densities of states for electrons and holes per band extrema and per spin direction is given by

$$\rho(E)=\frac{N_e 4\pi V\sqrt{E}}{(8\pi^3)(\hbar^2/2m^* m_0)^{3/2}}, \quad (6)$$

where N_e is the number of equivalent ellipsoids in the first Brillouin zone, the volume of the unit cell is $V=a_L^3$, a_L is the lattice constant, m^* is one of the effective masses listed in Table II for the appropriate band extrema, and m_0 is the free-electron mass. Because eight permutations of the wave vector in the (111) direction exist, there are eight-L subband ellipsoids with centers located near the boundary of the first Brillouin zone. Also, because six-permutations of the wave vector in the (100) direction exist, there are six-X subband ellipsoids with centers located near the boundary of the first Brillouin zone. Since about half of each ellipsoid is in the neighboring zone, the number of the equivalent subbands N_{cL} for the E_{cL} is four and the number of the equivalent subbands N_{eX} for the X subband is three.

In terms of a four-band model for room-temperature n-type GaSb, the total density-of-states $\rho_c(E)$ for the majority carrier electrons in n-type GaSb then becomes

$$\rho_c(E)=\rho_{c\Gamma}(E)+\rho_{cL}(E)+\rho_{cX}(E), \quad (7)$$

where $\rho_{c\Gamma}(E)$, $\rho_{cL}(E)$, and $\rho_{cX}(E)$ are the subband densities of states for the conduction Γ, L, and X subbands with effective masses of $m_{c\Gamma}$, m_{cL}, and m_{cX}, respectively. The density of states for the minority carrier holes is

$$\rho_v(E)=\rho_{v\Gamma}(E), \quad (8)$$

with an effective mass of $m_{v\Gamma}$.

III. RESULTS

Tables I and II contain the input parameters from Ref. 17 for the calculations of the Fermi energy as a function of the dopant donor density. We solve self-consistently, by means of an iterative procedure, Eq. (3) with Eqs. (6)–(8). The independent variable is the temperature T. The Fermi energy is varied for a given temperature and donor density until Eq. (3) is satisfied. Figure 1 presents the calculated Fermi energy data for 32 values of donor densities between 10^{16} and 10^{19} cm^{-3} with an acceptor compensation density of 10^{16} cm^{-3} and compares the compensated data reported here with the uncompensated data from Ref. 15. We see that for donor densities above 10^{17} cm^{-3} the effect of an acceptor compensation of 10^{16} cm^{-3} on the Fermi energy is negligible. Figure 2 for uncompensated GaSb and Fig. 3 for compensated GaSb give the total electron density and the electron densities in the conduction subbands at Γ, L, and X as functions of the Fermi energy. Figures 2 and 3 show that the electron density in the conduction X sub—is less than 10^{-3} times the total electron density. Because $m_{c\Gamma}\ll m_{cL}$ and E_{cL} is

Downloaded 11 Mar 2008 to 129.6.65.17. Redistribution subject to AIP license or copyright; see http://jap.aip.org/jap/copyright.jsp

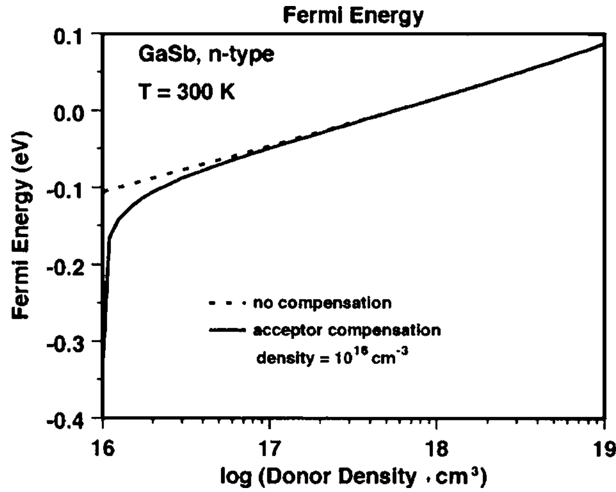

FIG. 1. The calculated Fermi energy for n-type GaSb at 300 K as a function of the donor density. The Fermi energy is relative to the majority conduction band edge at the Γ symmetry point in the first Brillouin zone.

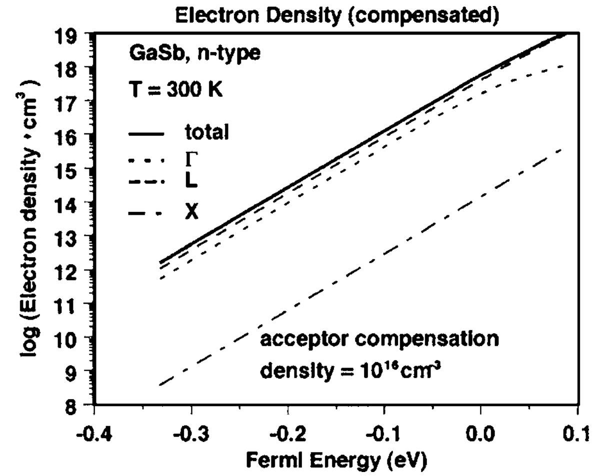

FIG. 3. The calculated electron densities for compensated GaSb in the conduction subbands at Γ, L, and X and the total electron density as functions of the Fermi energy. The Fermi energy is relative to the majority conduction band edge at the Γ symmetry point in the first Brillouin zone.

much closer to $E_{c\Gamma}$ than it is to E_{cX}, the electron density in the conduction L subband exceeds the electron density in the conduction Γ subband at room temperature. Figures 2 and 3 show that the majority of electrons is in the conduction L subband and that the density of electrons in the L subband approaches the total density of electrons as the donor density approaches 10^{19} cm^{-3}. Hence, even though GaSb is intrinsically a direct semiconductor, the results from Figs. 2 and 3 suggest that electrons for n-type GaSb in the vicinity of the Fermi surface will behave as though they have many characteristics of electrons in an indirect semiconductor.

Using the values for the subband edges and effective masses given in Table VII, page 5830, of Ref. 18 instead of the values given in Tables I and II of this paper leads to a variation in $\log_{10}(n\ \mathrm{cm}^{-3})$ at given Fermi energies of about 4% for electron densities between 10^{17} and 10^{19} cm^{-3}. The 4% uncertainties in $\log_{10}(n\ \mathrm{cm}^{-3})$ gives factors of 5–6 uncertainties in n.

Because the Raman experiments maybe sensitive to not only the total electron density but also to the electron densities in each of the three subbands, we give here the results for fitting the logarithm to the base 10 of the total electron density and the electron densities in each of the three conduction subbands at Γ, L, and X, n_Γ, n_L, and n_X, respectively, to polynomials in E_F, namely,

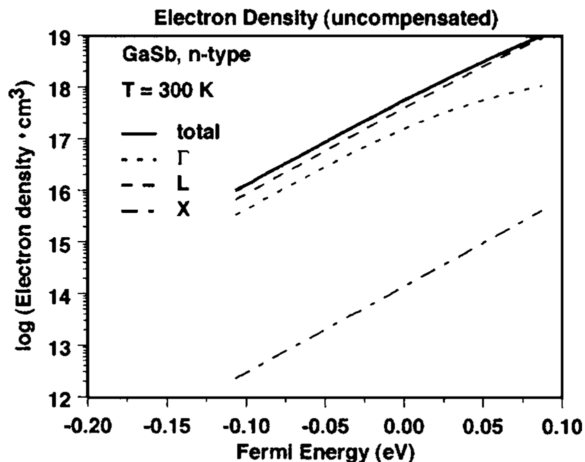

FIG. 2. The calculated electron densities for uncompensated GaSb in the conduction subbands at Γ, L, and X and the total electron density as functions of the Fermi energy. The Fermi energy is relative to the majority conduction band edge at the Γ symmetry point in the first Brillouin zone.

$$\log_{10}(n\ \mathrm{cm}^{-3}) = a_{t0} + a_{t1}E_F + a_{t2}E_F^2 + \cdots + a_{tl}E_F^l \ldots, \quad (9)$$

$$\log_{10}(n_\Gamma\ \mathrm{cm}^{-3}) = a_{\Gamma 0} + a_{\Gamma 1}E_F + a_{\Gamma 2}E_F^2 + \cdots + a_{\Gamma l}E_F^l \ldots, \quad (10)$$

$$\log_{10}(n_L\ \mathrm{cm}^{-3}) = a_{L0} + a_{L1}E_F + a_{L2}E_F^2 + \cdots + a_{Ll}E_F^l \ldots, \quad (11)$$

and

$$\log_{10}(n_X\ \mathrm{cm}^{-3}) = a_{X0} + a_{X1}E_F + a_{X2}E_F^2 + \cdots + a_{Xl}E_F^l \ldots . \quad (12)$$

We also give the analytic fit for inverse of Eq. (9), namely,

$$E_F = b_{t0} + b_{t1}N + b_{t2}N^2 + \cdots + b_{tl}N^l \ldots, \quad (13)$$

where $N = \log_{10}(n\ \mathrm{cm}^{-3})$. During the fitting analyses, we rely substantially on graphics and keep the number of fitting parameters to a minimum, subject to the constraint that the residual standard deviation S_{res} is acceptably small, i.e., $S_{\mathrm{res}} \leq 0.01$. The standard deviation is a measure of the "average" error in a fitted model and thereby is a metric for assessing the quality of the fit. A smaller S_{res} indicates a better fit. The residual standard deviation for a model $Y^f = f(Z)$ is

$$S_{\mathrm{res}} = \sqrt{\left[\sum_{j=1}^{N} (Y_j - \bar{Y}_j^f)^2/(N-P)\right]}, \quad (14)$$

where Y_j are the calculated data values, $\bar{Y}_j^f$ are the predicted values from the fitted model, N is the total number of data points (here $N=32$), and P is the total number of parameters to be fitted in the model. We use the NIST-developed DATAPLOT software for both the exploratory graphics and for the statistical analyses.[19]

Downloaded 11 Mar 2008 to 129.6.65.17. Redistribution subject to AIP license or copyright; see http://jap.aip.org/jap/copyright.jsp

TABLE III. The four-fitting parameters for a cubic polynomial fit Eq. (9) of the theoretical calculation for the total electron density in compensated n-type, zinc-blende GaSb at 300 K as a function of the Fermi energy relative to the bottom of the conduction Γ subband. This cubic polynomial fit, which represents the theoretical results for Eq. (3), is valid only when −0.333 eV $\leqslant E_F \leqslant$ 0.0871 eV. The ratio is the estimated value divided by the estimated standard deviation. The residual standard deviation is S_{res}=0.0057. The compensation acceptor density is 10^{16} cm^{-3}.

Fitting parameter	Estimated value	Estimated standard deviation	Units	Ratio
a_{t0}	17.7476	0.1448×10^{-2}		0.12×10^{5}
a_{t1}	15.5232	0.1827×10^{-1}	eV^{-1}	0.85×10^{3}
a_{t2}	−9.96752	0.2817	eV^{-2}	-3.5×10^{1}
a_{t3}	−19.6469	0.8066	eV^{-3}	-2.4×10^{1}

TABLE V. The four-fitting parameters for a cubic polynomial fit Eq. (11) of the theoretical calculation for the L subband electron density in compensated n-type, zinc-blende GaSb at 300 K as a function of the Fermi energy relative to the bottom of the condition Γ subband. This cubic polynomial fit, which represents the theoretical results for Eq. (3), is valid only when −0.333 eV $\leqslant E_F \leqslant$ 0.0871 eV. The ratio is the estimated value divided by the estimated standard deviation. The residual standard deviation is S_{res}=0.0088. The compensation acceptor density is 10^{16} cm^{-3}.

Fitting parameter	Estimated value	Estimated standard deviation	Units	Ratio
a_{L0}	17.6047	0.2207×10^{-2}		0.80×10^{4}
a_{L1}	16.2729	0.2785×10^{-1}	eV^{-1}	0.58×10^{3}
a_{L2}	−5.47732	0.4293	eV^{-2}	−13
a_{L3}	−11.9510	1.229	eV^{-3}	−9.7

Tables III, V, and VI give the fitting parameters for the cubic $l=3$ polynomial fits to $\log_{10}(n\ \mathrm{cm}^{-3})$, $\log_{10}(n_L\ \mathrm{cm}^{-3})$, and $\log_{10}(n_X\ \mathrm{cm}^{-3})$ as shown, respectively, in Eqs. (9), (11), and (12), and the associated residual standard deviations S_{res}. Table IV gives the fitting parameters for the quartic cubic $l=4$ polynomial fit to $\log_{10}(n_\Gamma\ \mathrm{cm}^{-3})$ as shown in Eq. (10). For the conduction Γ subband, $S_{res}=0.016$ when $l=3$, whereas $S_{res}=0.002$ when $l=4$. In general, the values of S_{res} decrease monotonically with increasing number l of terms in these polynomials. But, care must be taken to avoid fitting noise in data sets. The general guideline for many data sets is that when the absolute value of the ratio R of the estimated parameter value divided by its estimated standard deviation is less than about 2, then the rate of decrease in S_{res} with increasing l tends to decrease. Because the changes in values of S_{res} between $l=3$ and $l=4$ are not experimentally significant, we use the fitting parameters for the cubic $l=3$ case in Eqs. (9), (11), and (12) and for the quartic case $l=4$ for Eq. (10). Also, when the ratios R for the parameters a_4 when $l=4$ are less than about −2, such values for R mean typically that proceeding with higher l values probably is not warranted. Figure 2 compares the calculated electron densities as functions of the Fermi energy with the fitting results from Eqs. (9)–(12) for the polynomials given in Tables III–VI. Figure 2 shows that the pairs of curves (calculated and fitted) for each of the electron densities n, n_Γ, n_L, and n_X, lie on top of one another to within the linewidths of each curve. Also, since the screening radii for the carriers from Eq. (2) are not needed when interpreting the proposed measurements considered here, the corresponding screening radii are not presented in this paper.

Table VII gives the fitting parameters for the cubic $l=3$ polynomial fit of the Fermi energy E_F in terms of $N=\log_{10}(n\ \mathrm{cm}^{-3})$ as shown in Eq. (13).

IV. CONCLUSIONS

The results in Sec. III are consistent with the findings of experimental work reported in the literature, such as Refs. 20 and 21, concerning the relative distributions of electrons among the conduction Γ, L, and X subbands. Interpreting experiments for GaSb requires at least a three-band model and under some conditions may require a four-band model. Even though GaSb is intrinsically a direct semiconductor, our results show that electrons for n-type GaSb in the vicinity of the Fermi surface will have some characteristics that are similar to those for electrons in an indirect semiconductor.

The sensitivity analyses presented in Sec. III compare results based on input parameters from Refs. 17 and 18 and suggest that the value of E_{cL} must be determined with more certainty in order to improve the accuracy and precision of electron concentrations extracted from Raman spectra by using self-consistent first-principles methods. However, there

TABLE IV. The five-fitting parameters for a quartic polynomial fit Eq. (10) of the theoretical calculation for the Γ subband electron density in compensated n-type, zinc-blende GaSb at 300 K as a function of the Fermi energy relative to the bottom of the conduction Γ subband. This quartic polynomial fit, which represents the theoretical results for Eq. (3), is valid only when −0.333 eV $\leqslant E_F \leqslant$ 0.0871 eV. The ratio is the estimated value divided by the estimated standard deviation. The residual standard deviation is S_{res}=0.007. The compensation acceptor density is 10^{16} cm^{-3}.

Fitting parameter	Estimated value	Estimated standard deviation	Units	Ratio
$a_{\Gamma 0}$	17.1963	0.1740×10^{-2}		0.99×10^{4}
$a_{\Gamma 1}$	13.3495	0.4258×10^{-1}	eV^{-1}	0.31×10^{3}
$a_{\Gamma 2}$	−32.8289	0.3877	eV^{-2}	−85
$a_{\Gamma 3}$	−124.953	5.638	eV^{-3}	−22
$a_{\Gamma 4}$	−162.603	13.86	eV^{-3}	−12

TABLE VI. The four-fitting parameters for a cubic polynomial fit Eq. (12) of the theoretical calculation for the X subband electron density in compensated n-type, zinc-blende GaSb at 300 K as a function of the Fermi energy relative to the bottom of the conduction Γ subband. This cubic polynomial fit, which represents the theoretical results for Eq. (3), is valid only when −0.333 eV $\leqslant E_F \leqslant$ 0.0871 eV. The ratio is the estimated value divided by the estimated standard deviation. The residual standard deviation is S_{res}=0.000 02. The compensation acceptor density is 10^{16} cm^{-3}.

Fitting parameter	Estimated value	Estimated standard deviation	Units	Ratio
a_{X0}	14.1542	0.5993×10^{-5}		0.24×10^{7}
a_{X1}	16.7997	0.7561×10^{-4}	eV^{-1}	0.22×10^{6}
a_{X2}	$0.801\,067\times 10^{-3}$	1.1166×10^{-2}	eV^{-2}	0.69
a_{X3}	$0.609\,853\times 10^{-2}$	0.3338×10^{-1}	eV^{-3}	1.8

Downloaded 11 Mar 2008 to 129.6.65.17. Redistribution subject to AIP license or copyright; see http://jap.aip.org/jap/copyright.jsp

TABLE VII. The four-fitting parameters for a cubic polynomial fit given in Eq. (13) to the theoretical calculation for the Fermi energy relative to the bottom of the conduction Γ subband in compensated n-type, zinc-blende GaSb at 300 K as a function of $N=\log_{10}(n\ \mathrm{cm}^{-3})$, where n is the total electron density in cm^{-3}. This cubic polynomial fit, which represents the theoretical results for Eq. (3), is valid only when $-0.333\ \mathrm{eV} \leq E_F \leq 0.0871$ eV. The ratio is the estimated value divided by the estimated standard deviation. The residual standard deviation is $S_{\mathrm{res}}=0.000\,53$. The compensation acceptor is $10^{16}\ \mathrm{cm}^{-3}$.

Fitting parameter	Estimated value	Estimated standard deviation	Units	Ratio
b_{t0}	−2.082 42	0.6908×10^{-1}	eV	−30.15
b_{t1}	0.268 479	0.1342×10^{-1}	eV	20.01
b_{t2}	$-0.140\,708\times10^{-1}$	0.8581×10^{-3}	eV	−16.40
b_{t3}	$0.312\,985\times10^{-3}$	0.1809×10^{-4}	eV	17.30

maybe large enough uncertainties in the values of GaSb materials properties other than E_{cL} that make it difficult to identify the largest sources of error at this time.

ACKNOWLEDGMENTS

We acknowledge many discussions with James Maslar and Wilbur Hurst concerning physical models for interpreting Raman scattering measurements. We thank Alan Heckert for guidance in using DATAPLOT. We thank James Filliben for help in obtaining the closed-form analytic expressions for carrier densities from numerical tabulations of theoretical calculations. We benefited substantially from having access to computers in the NIST Information Technology Laboratory (ITL) and from support given by ITL staff members, particularly, Judith Devaney and James Sims.

[1] *2003 International Technology Roadmap for Semiconductors* (International SEMATECH, Austin, Texas, 2003); http://public.itrs.net/Files/2003ITRS/Home2003.htm

[2] *2002 NEMI Technology Roadmaps and 2003 NEMI Research Priorities* (National Electronics Manufacturing Initiative, Inc., Herndon, VA, 2003); http://www.nemi.org/roadmapping/00RoadFormWeb.html

[3] *Chemical Industry R&D Roadmap for Nanomaterials By Design: From Fundamentals to Function* (Chemical Industry Vision 2020 Technology Partnership, Baltimore, MD, 2003); http://www.chemicalvision2020.org/nanomaterialsroadmap.html

[4] J. Ibáñez, R. Cuscó, and L. Artús, Phys. Status Solidi B **223**, 715 (2001).

[5] G. Abstreiter, M. Cardona, and A. Pinczuk, *Light Scattering by Free Carrier Excitations in Semiconductors*, Light Scattering in Solids Vol. IV, edited by M. Cardona and G. Güntherodt (Springer, New York, 1984), Chap. 2, pp. 5–150.

[6] S. Ernst, A. R. Goñi, K. Syassen, and M. Cardona, Phys. Rev. B **53**, 1287 (1996).

[7] R. Cuscó, L. Artús, S. Hernández, J. Ibáñez, and M. Hopkinson, Phys. Rev. B **65**, 035210 (2001).

[8] W. Richter, U. Nowak, H. Jürgensen, and U. Rössler, Solid State Commun. **67**, 199 (1988), See Eq. (10), p. 201, therein.

[9] L. Artus, R. Cusco, J. Ibanez, N. Blanco, and G. Gonzalez-Diaz, Phys. Rev. B **60**, 5456 (1999).

[10] J. F. Chen and A. Y. Cho, J. Appl. Phys. **70**, 277 (1991).

[11] A. Sagar, Phys. Rev. **117**, 93 (1960).

[12] P. C. Mathur and Sushil Hain, Phys. Rev. B **19**, 3159 (1979).

[13] S. Subbanna, G. Tuttle, and H. Kroemer, J. Electron. Mater. **17**, 297 (1988).

[14] H. S. Bennett, J. Appl. Phys. **83**, 3102 (1998).

[15] H. S. Bennett and Howard Hung, J. Res. Natl. Inst. Stand. Technol. **108**, 193 (2003).

[16] J. S. Blakemore, J. Appl. Phys. **53**, R123 (1982).

[17] A. Ya. Vul, in *Handbook Series on Semiconductor Parameters*, edited by M. Levinshtein, S. Rumyantsev, and M. Shur (World Scientific, Singapore, 1996), Vol. I pp. 125–146.

[18] I. Vurgaftman, J. R. Meyer, and L. R. Ram-Mohan, J. Appl. Phys. **89**, 5815 (2001).

[19] J. J. Filleben and A. N. Heckert, the DATAPLOT software for graphics and detailed statistical analyses runs on both UNIX and WINTEL platforms. It has both command-line versions and graphical user interface (GUI) versions. It is available by downloading from http://www.itl.nist.gov/div898/software/dataplot/. In addition, the NIST-SEMATECH Engineering Statistics Handbook at http://www.itl.nist.gov/div898/handbook/ is based in part on DATAPLOT. This latter WWW site has tutorials that explain in some detail the statistical analysis methods used in this paper.

[20] A. Baraldi, F. Colonna, C. Ghezzi, R. Magnanini, A. Parisini, L. Tarricone, A. Bosacchi, and S. Franchi, Semicond. Sci. Technol. **11**, 1656 (1996).

[21] V. W. L. Chin, Solid-State Electron. **38**, 59 (1995).

Downloaded 11 Mar 2008 to 129.6.65.17. Redistribution subject to AIP license or copyright; see http://jap.aip.org/jap/copyright.jsp